PHYSICAL REVIEW E VOLUME 58, NUMBER 2 AUGUST 1998

Free particle chaotic scattering off two oscillating disks

A. Antillón,[1] Jorge V. José,[2,3] and T. H. Seligman[1]
[1] *Instituto de Física, Universidad Nacional Autónoma de México, Apartado Postal 48-3, 62251 Cuernavaca, Morelos, Mexico*
[2]*Physics Department and Center for the Interdisciplinary Research on Complex Systems, Northeastern University, Boston, Massachusetts, 02115**
[3]*Instituto de Física, Universidad Nacional Autónoma de México, Apartado Postal 20-364, 01000 México Distrito Federal, México*

(Received 2 March 1998)

We investigate the two-dimensional classical dynamics of the scattering of point particles by two periodically oscillating disks. The dynamics exhibits regular and chaotic scattering properties, as a function of the initial conditions and parameter values of the system. The energy is not conserved, since the particles can gain and lose energy from the collisions with the disks. We find that for incident particles whose velocity is on the order of the oscillating disk velocity, the energy of the exiting particles displays nonmonotonic gaps of allowed energies, and the distribution of exiting particle velocities shows significant fluctuations in the low energy regime. We also considered the case when the initial velocity distribution is Gaussian, and found that for high energies the exit velocity distribution is Gaussian with the same mean and variance. When the initial particle velocities are in the irregular regime the exit velocity distribution is Gaussian, but with a smaller mean and variance. The latter result can be understood as an example of stochastic cooling. In the intermediate regime the exit velocity distribution differs significantly from Gaussian. A comparison of the results presented in this paper to previous chaotic static scattering problems is also discussed. [S1063-651X(98)14408-2]

PACS number(s): 05.45.+b, 95.10.−a

I. INTRODUCTION

The study of nonlinear systems capable of exhibiting chaotic behavior has been an intensive area of research in the last 15 years. This research was initiated about a century ago by the work of Henri Poincaré, who studied the motion of three gravitationally interacting bodies. Most of the work done on this subject has focused on bounded systems. On the other hand, many experimental techniques involve scattering processes. In contrast to bounded systems, where the particle's trajectories remain forever inside the range of interaction, in a scattering process an incoming particle ''feels'' the interaction potential only for a finite amount of time and eventually exits the interaction region [1–11]. In the general description of a scattering process, we have an input trajectory into a region of nontrivial dynamics called the scattering region, and an output trajectory away from this region. We can think of the scattering process as a map that transforms an incoming trajectory into an outgoing one. Only relatively recently has it been realized that a scattering processes from a general scattering potential, often without a simple geometric symmetry, can have rather complicated dependencies between the incoming and outgoing trajectories. This means that, by very slightly changing the initial conditions that define the incoming trajectory, the outgoing trajectory will have rather large fluctuations. The idea that *chaotic scattering* can play an important role in various problems in physics became widely accepted after the seminal work of Petit and Hénon [4] (see also Ref. [1]).

Most previous chaotic scattering studies have assumed a stationary scattering region, i.e., fixed in time (for an exception, see Ref. [12]). In this paper we present results from a dynamical study of the scattering of particles from a time-dependent oscillatory interaction potential, which consists of two circular disks that oscillate periodically in time. The static two-disk problem was recently shown to be analytically integrable [11], (hereafter we call this work I). In this paper we build our nonequilibrium dynamical study based upon the results obtained in I.

Our model can conceivably be produced in very low temperature experiments, where a pair of circular quantum dots is generated by a gate voltage that can vary their radius periodically in time. Ballistic transport experiments in mesoscopic systems have raised the possibility of directly studying chaotic billiards, where the addition of external fields can yield results that are expected to account for certain aspects of unusual related experimental results [13–20]. Some of the transport results seen in experiments are surmised to have classical related explanations [21–26]. The geometry of microjunctions [13] and antidot-lattices [14,15] can be described by models that consist of circular scattering disks. For the above reasons, in this paper we will focus on the scattering of a particle from two oscillating classical hard-disk billiards. Here we concentrate on the classical dynamics of this model, and leave the very interesting quantum case for a future study.

The outline of the paper is the following: In Sec. II, we introduce the model considered in this paper, together with its main physical properties. In Sec. III, we derive a scattering map associated with our problem. In Sec. IV, we present and discuss the bulk of our results. Finally, in Sec. V, we provide a short summary of the results and the perspectives for the future.

II. DEFINITION OF THE PROBLEM

We consider the motion of a unit mass particle restricted to moving on the plane. The particle elastically collides with

---

*Permanent address.

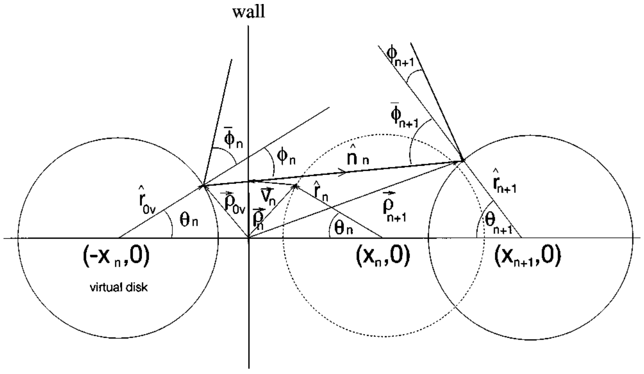

FIG. 1. This figure defines the two-disk periodically oscillating model studied in this paper. The model is replaced and studied by the one oscillating disk and a fixed wall. The figure shows a dotted line disk with a center at $X_n=X(t_n)$, and a continuous line circle at the right of the wall with center at $X_{n+1}=X(t_{n+1})$. The disk on the left of the wall represents the image of the dotted line disk. Variables with a subindex n are evaluated at time t_n.

two hard disks that oscillate periodically in time. The initial velocity of the particle changes as a function of time due to the energy exchange after each collision with the disks. As we discuss below, depending on the initial conditions the particle will spend a certain amount of *dwell time* in the interaction region, after which time it will exit upwards or downwards. It is the complexity of this motion that we will carefully describe below.

Here we will follow the approach presented in I [11], including its notation. The reader should check this reference for further details on the formulation of the static problem. In Fig. 1, we show the two disks on the plane. The radii of both disks are normalized to 1. Their centers are separated by a time-dependent distance $R(t)>2$. One convenient way to study this problem, as pointed out in I, is by replacing the system by one disk and one rigid wall placed at the symmetry axis of the two-disk problem. This is the representation of the model we study in this paper.

Two-disk oscillating model

The model we consider here is in some sense the scattering two-dimensional extension of the well studied *bound Fermi acceleration* model [27,28]. This model is defined by a free particle inside a rigid one-dimensional box, with one wall fixed and the other one periodically oscillating in time. The Fermi model was one of the first two degrees of freedom problems studied, which exhibited a transition from regular to chaotic behavior as a function of the oscillating wall motion. For a linear saw-tooth time-dependent wall oscillation, the particle dynamics is regular. Having a linear time dependence implies a constant oscillating wall velocity. When the oscillation is nonlinear in time, there is acceleration in the wall motion, and one can then have nontrivial dynamics, with a transition between regular to fully chaotic behavior. In this paper, without loss of generality, we consider the simplest nonlinear piecewise quadratic time-dependent disk oscillation shown in Fig. (2). In this case we represent the motion of the disk center by

$$X(t)=\tilde{A}t^2+\tilde{B}t+\tilde{C}. \tag{1}$$

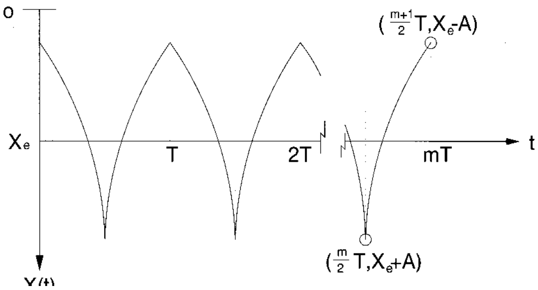

FIG. 2. Here $X(t)$ denotes the oscillating wall model about the equilibrium position X_e in the range $[X_e-A,X_e+A]$, with amplitude A. The parameter m labels the oscillation segment with fixed value in the time interval $((m/2)\,T,[(m+1)/2]\,T)$. The relation between time t and m is given in Eq. (2). The figure is drawn for $\Phi_0=0$.

Here the constants $\tilde{A}$, $\tilde{B}$, and $\tilde{C}$ are fixed for a half period, and they have different values for different half periods. The motion of the disk center (the other disk is the mirror image of this one) is given by Eq. (1), the modulus the oscillation disk period T.

In our analysis, for calculational convenience, we chose to treat the problem in the following way. We label by the integer m each continuous piece of the disk oscillation. The time t and m are then related by the expression

$$m=\left[\left[\frac{2(t+\Phi_0/\omega)}{T}\right]\right], \tag{2}$$

where [[ ]] denotes the nearest lower integer. The m parameter will have a fixed value for time t in the time interval $(m/2)T\leqslant t\leqslant[(m+1)/2]T$. Here $\omega=2\pi/T$ is the oscillation frequency, and Φ_0 is the initial oscillation phase. The specific expressions that define the parameters $\tilde{A}$, $\tilde{B}$, and $\tilde{C}$ are given in the Appendix.

We have now defined the time dependence of the oscillating disk. Next we use the relevant results given in I, noting that the incidence-reflect symmetry in our case is changed by the oscillation of the disk.

1. Collision Time

We start by calculating the time elapsed between two successive collisions of the particle with the disk. We need this time to calculate the new velocity vector, by means of a velocity transformation to the system where the disk is at rest. We deduce from Fig. 1 that the position of the colliding particle is given by

$$\vec{\rho}(t_{n+1})=\vec{\rho}_{n+1}=\vec{\rho}_{nv}+\vec{v}_{nv}(t-t_n), \tag{3}$$

where t_n is the previous collision time, and the subindex v denotes a *specular variable.* To clarify the meaning of *specular,* consider for example, the one associated with $\vec{\rho}_n(t)=(x_n,y_n)$, which gives

$$\vec{\rho}_{nv}=(x_{nv},y_{nv})=(-x_n,y_n)=(-X_n+\cos\,\theta_n,\sin\,\theta_n), \tag{4}$$

and the velocity

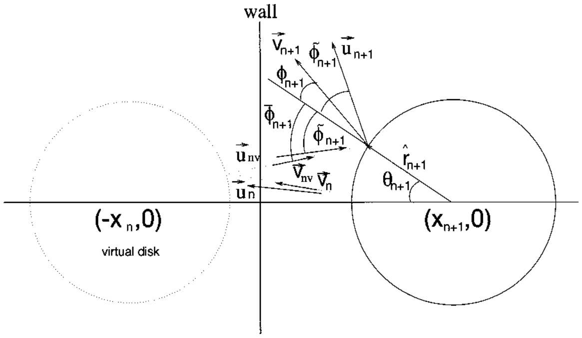

FIG. 3. This figure is used in the derivation of the velocities map. The relative velocities before and after the collision have the same angle with respect to the normal to the disk, but the velocity itself has two different angles. See text for the definition of the variables in this figure.

$$\begin{aligned}\vec{v}_{nv}&=(v_{nvx},v_{nvy})=(-v_{nx},v_{ny})\\&=[v_n\cos(\theta_n-\phi_n),v_n\sin(\theta_n-\phi_n)].\end{aligned}\tag{5}$$

The new collision point $\vec{\rho}_{n+1}=(x_{n+1},y_{n+1})$, at the new collision time t_{n+1}, must lie on the circumference given by the equation

$$[x_{n+1}-X(t_{n+1})]^2+y_{n+1}^2=1.\tag{6}$$

Evaluating Eq. (1) at $t=t_{n+1}$, and substituting it in Eq. (6), we obtain the quartic equation for t_{n+1},

$$a_4t_{n+1}^4+a_3t_{n+1}^3+a_2t_{n+1}^2+a_1t_{n+1}+a_0=0,\tag{7}$$

where the expression for the parameters a_0, a_1, a_2, a_3 and a_4, are explicitly given in Eq. (A2).

We can obtain t_{n+1} as a function of t_n using Eq. (7) and Eq. (A2). Once we know t_{n+1}, the collision point on the disk can be determined from Eq. (3) as

$$x_{n+1}=-x_n-v_{nx}(t_{n+1}-t_n),y_{n+1}=y_n+v_{ny}(t_{n+1}-t_n),\tag{8}$$

and then, using Eq. (6), the disk will be located at

$$X_{n+1}=x_{n+1}+\sqrt{1-y_{n+1}^2}\tag{9}$$

2. Disk velocity map

To calculate the velocity of the disk, $\vec{V}_{n+1}$ at the new collision time, we take the time derivative of Eq. (1) that gives

$$\vec{V}(t)=(\dot{X}(t),0)=(2\tilde{A}t+\tilde{B},0),\tag{10}$$

and consequently

$$\vec{V}_{n+1}=\vec{V}(t_{n+1})=(2\tilde{A}t_{n+1}+\tilde{B},0),\equiv(V_{n+1},0)\tag{11}$$

which is fully determined since t_{n+1} is known from Eq. (7). To determine the velocity of the particle, $\vec{v}_{n+1}$, we introduce the relative particle velocity (see Fig. 3) with respect to the disk as

$$\vec{u}=\vec{v}-\vec{V}.\tag{12}$$

Then

$$\vec{u}_{nv}\wedge\hat{r}_{n+1}=P\hat{k},\tag{13}$$

where

$$P=[(X_{n+1}-x_{n+1})u_{ny}-y_{n+1}u_{nx}],\tag{14}$$

and

$$u_{nx}=v_{nx}+V_{n+1},\quad u_{ny}=v_{ny},\tag{15}$$

with the normal unit vector $\hat{k}\|\hat{z}$, as seen in the figure. One can also show that

$$\vec{u}_{n+1}\wedge\hat{r}_{n+1}=[u_{n+1x}y_{n+1}-u_{n+1y}(x_{n+1}-X_{n+1})]\hat{k}.\tag{16}$$

From these two equations, we obtain

$$u_{n+1y}=\bar{P}-Qu_{n+1x},\tag{17}$$

with

$$\bar{P}=\frac{P}{X_{n+1}-x_{n+1}}\quad\text{and}\quad Q=\frac{y_{n+1}}{X_{n+1}-x_{n+1}}.\tag{18}$$

We also have the conservation of the velocity magnitude, which in the coordinate frame where the disk is at rest is given by

$$u_{n+1x}^2+u_{n+1y}^2=u_n^2.\tag{19}$$

Using Eq. (15) in the last equation we obtain

$$u_{n+1x}=\frac{\bar{P}Q-\sqrt{\bar{P}^2Q^2-(1+Q^2)(\bar{P}^2-u_n^2)}}{1+Q^2},\tag{20}$$

with an appropriately chosen minus sign in the square root. We now go back to Eq. (15) to find u_{n+1y}. This allows us to obtain the velocity of the particle after the collision through the expressions

$$v_{n+1x}=u_{n+1x}+V_{n+1}\quad\text{and}\quad v_{n+1y}=u_{n+1y}.\tag{21}$$

III. SCATTERING MAP

Following the notation of I, we can obtain the scattering map associated with this dynamical system. Since the derivation of our map is completely analogous to the one given there, we can directly write down the final expressions stating a few differences proper to our problem. The map derived in I is

$$\phi_{n+1}=\sin^{-1}\left[\frac{v_n}{v_{n+1}}[\sin\phi_n+\bar{R}\sin(\theta_n-\phi_n)]\right],\tag{22}$$

$$\theta_{n+1}=\sin^{-1}[\sin\theta_n+\lambda\sin(\theta_n-\phi_n)].\tag{23}$$

In our case $\bar{R}=X_n+X_{n+1}$, and

$$\begin{aligned}\lambda=&\bar{R}\cos(\theta_n-\phi_n)-\cos\phi_n\\&-\sqrt{[\cos\phi_n-\bar{R}\cos(\theta_n-\phi_n)]^2-\bar{R}^2+2\bar{R}\cos\theta_n}.\end{aligned}\tag{24}$$

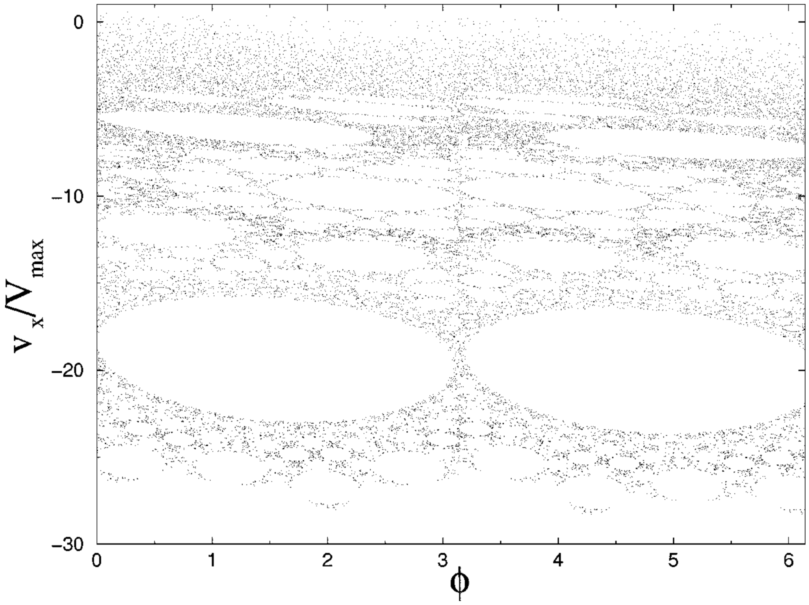

FIG. 4. Phase space results for a limit close to the Fermi acceleration one-dimensional model. Here v_x is the x component of the particle velocity, normalized by the disk velocity $V_{\max}$. The particle will eventually sense the disk two-dimensional curvature, and the resonance structures, as compared to the Fermi model, will change. The plot has 74 238 points obtained from 17 particles with different initial velocities.

The initial conditions (θ_0, ϕ_0) in this map are obtained from the parameters set at time $t=0$. If we take the initial particle position as $(x_{\bar{0}}, y_{\bar{0}})$, the angle α between the initial velocity $\vec{v}_{\bar{0}}$ and the horizontal gives

$$\phi_0 = \sin^{-1}\left[\frac{v_{\bar{0}}}{v_0}[(X_0 - x_{\bar{0}})\sin\alpha + y_{\bar{0}}\cos\alpha]\right], \tag{25}$$

$$\theta_0 = \sin^{-1}(y_{\bar{0}} + \lambda_{\bar{0}}\sin\alpha). \tag{26}$$

In Eq. (25), $\vec{v}_0$ is given by $\vec{v}_0 = \vec{u}_0 + \vec{V}_0$, and $\vec{u}_0$ by

$$u_{0x} = \frac{\bar{R}S - \sqrt{\bar{R}^2 S^2 - (1+S^2)(\bar{R}^2 - u_{\bar{0}}^2)}}{1+S^2}, \tag{27}$$

$$u_{0y} = \bar{R} - S u_{0x}, \tag{28}$$

where

$$\bar{R} = \frac{R}{X_0 - x_0} \quad \text{and} \quad S = \frac{y_0}{X_0 - x_0}, \tag{29}$$

$$R = (X_0 - x_0)u_{\overline{0y}} + y_0 u_{\overline{0x}} u_{\overline{0x}} = v_{\overline{0x}} - V_0 \quad \text{and} \quad u_{\overline{0y}} = v_{\overline{0y}}. \tag{30}$$

The results derived in this section used a polar coordinates representation that has several advantages for the geometric analysis described here. When iterating the map numerically, however, the polar coordinate representation is somewhat cumbersome, and for that reason we found it more convenient to carry out the iterations in Cartesian coordinates. This is what we did to obtain the results described in Sec. IV.

IV. RESULTS

In this section we discuss the bulk of our numerical results. We provide typical results for a regime of interesting physical parameters. To check our analysis, we looked at the Fermi acceleration limit of our problem, which corresponds to having the two disks quite close to each other and with the particle initial conditions along the disks axis, so that the particle does not ''notice'' the disks curvature. We reproduced the Fermi accelerator model results by choosing the parameters for the equilibrium position of the disk center, X_e, the amplitude of oscillation, A, the time oscillation period T, and the free space distance between the wall and the disk, close to the values given in Refs. [27,28]. The phase space plots obtained correspond well to the known Fermi accelerator results, i.e., chaotic behavior for low velocities, and several sets of resonant islands for higher velocities.

After this test we chose a separation between the wall and disk large enough so that the particle dynamics sensed the curvature of the disks. Of course, if the separation distance is too large, the particle will hardly collide with the disk and the dynamics becomes trivial. The interesting parameter ranges are the ones which allow a large number of particle collisions with the oscillating disk and the wall. A typical phase space plot is shown in Fig. 4, for several particle initial conditions. The parameters considered satisfy the necessary condition to have a large number of particle collisions with the oscillating disk. In the units where the radius of the disk is 1, we took the parameters: $(X_e, 0) = (1.000\,097, 0)$, $A = 1.6\times10^{-6}$, $T = 7.6\times10^{-5}$, $\Phi_0 = 0$, and the acceleration parameter $\tilde{A} = 4716.085$. We considered a set of 2000 particle initial conditions, which we may as well call a beam of 2000 particles, each one sent from the origin into the scattering region with an angle $\alpha = 6\times10^{-2}$ radians with respect to the x axis. We varied the velocities of the particles be-

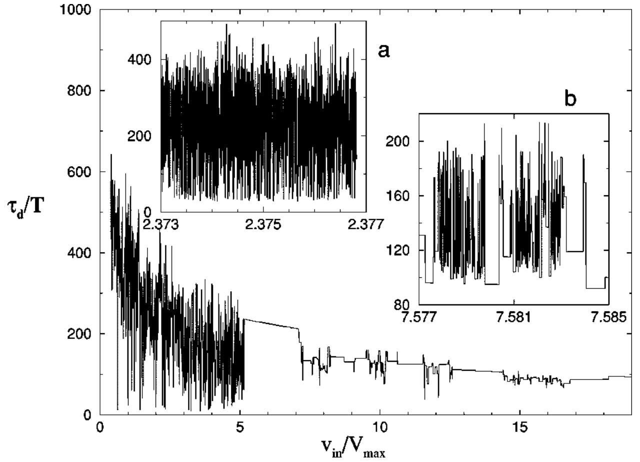

FIG. 5. Dwell time τ_d as a function of the normalized incident velocity $v_{\rm in}$. In inset (a) we show amplified results about $v_{\rm in} = 2.375$. We see that the low energy particles have an irregular behavior with a fractal-like character. Velocities higher than 5.5 have a mixture of regular and irregular behaviors. In inset (b) we show a further amplification around velocities close to 7.581. Each picture is drawn from results of 2000 initial conditions.

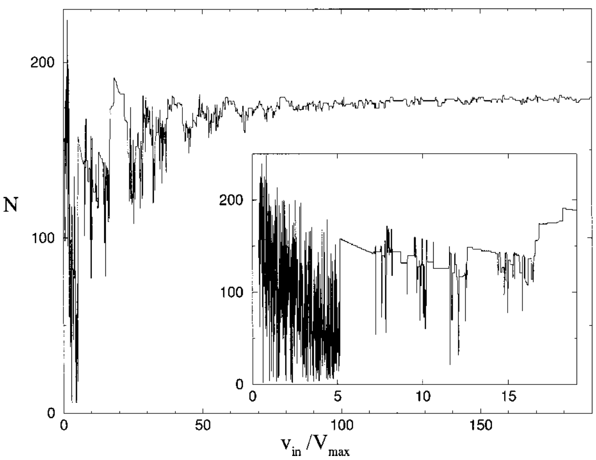

FIG. 7. Here we show the dependence between N and $v_{\rm in}/V_{\rm max}$. The main plot and the inset show the same general behavior as that of Fig. 5, with the irregular behavior in the same range of input velocities. For large velocities, N is basically constant. This means that the disk motion has little effect on the particle velocities. Each picture was done with 2000 particles.

tween 0.1 and 5.0, chosen from a uniform random distribution.

In Fig. 5 we show the delay, or *dwell time*, τ_d, as a function of the initial energy (velocity) of the incident particles. For low energies we observe a very irregular behavior in τ_d. In fact, this behavior is rather close to a fractal, as can be seen by zooming in a given interval of energies, as shown in the left inset. We also note that for initial velocities larger that 5.5, there is a mixture of regular and irregular zones. When we amplify one of the irregular regions, we can again see the fractal character of the results (see the inset on the right). For larger energies than the ones shown here, we found that τ_d tends to a constant value. This is what we would expect for large energies since the particle essentially sees the disk as stationary.

It is interesting to use the data of Fig. 5 to construct the histogram of dwell times shown in Fig. 6. The main histogram has two representative contributions. One comes from the irregular zone and the other one from the semiregular component, as shown in the two insets in the figure. The upper inset corresponds to the irregular region, and the lower one to the semiregular zone. The main histogram shows one peak close to a τ_d of about 100 and the other one close to 200, which correspond to the peaks seen in the insets. The bin size used in all the histograms shown are around 3% of the full range. In Fig. 7 we show the number of collisions with the disk versus the incoming velocity. The general be-

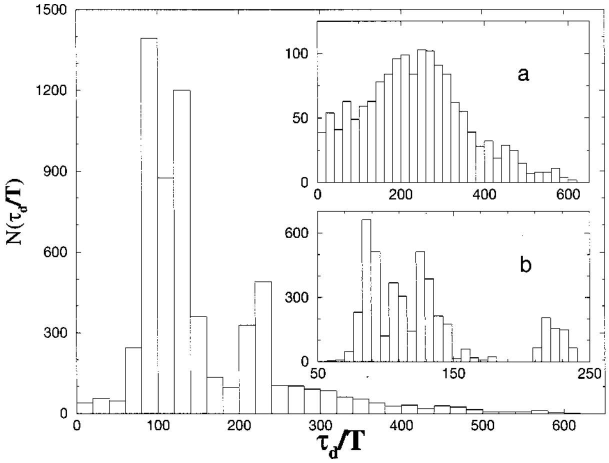

FIG. 6. Dwell time histogram $N(\tau_d/T)$ for data like the one shown in Fig. 5, except that here we used 6000 particles instead of the 2000 used in Fig. 5. The two noticeable peaks are due to the contributions from the irregular and semiregular zones, which correspond to the data shown in insets (a) and (b), respectively. The number of particles used to obtain the histograms was 2000. The bin size in the three histograms is around 3% of the full range in each plot.

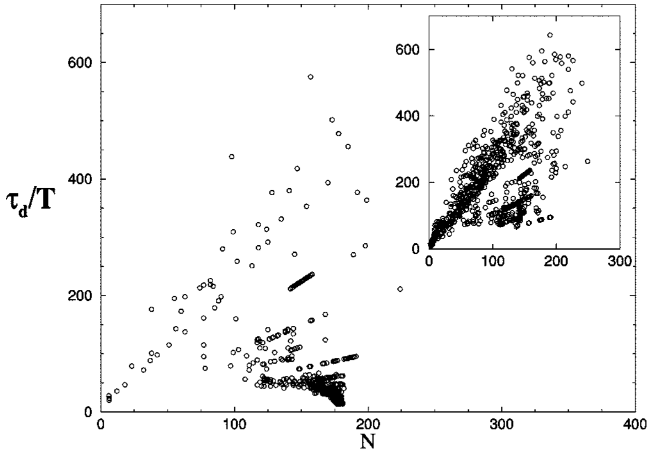

FIG. 8. Here we show a plot of τ_d vs N. We note that there is no clear relationship between these two variables. The general behavior of both plots are similar to the ones shown in Figs. 5 and 7. Note that for low $v_{\rm in}$ (irregular region), their dependence is irregular. The number of points taken was 2000. We see that when the input velocity is outside the irregular region, all the particles are concentrated in a black zone in the figure. This means the near independence of τ_d and N with respect to the input velocity.

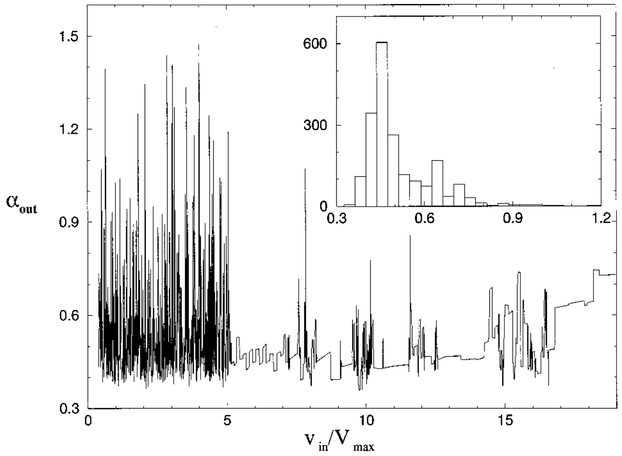

FIG. 9. Exit angle α_{out} as a function of v_{in}/V_{max}. The low velocity region again displays an irregular behavior for the exit angle. The inset in the figure for the preferred exit angle has a peak around 0.45 rad.

havior is very similar to that in Fig. 5, however, the explicit relationship is complicated. This can also be seen from Fig. 8, which we shall discuss in the next paragraph. In Fig. 7 we note, in particular, the irregular behavior in the same regions of incident velocities. As we increase the initial energy, the number of collisions reach a plateau, which is because the disk appears to be at rest. In the inset we used the same number of particles as used in the main figure, but the range of velocities is smaller, so as to allow us to see the results in more detail.

In Fig. 8 we display the dwell time vs the number of collisions, N, to see if there is a simple relation between them. The input velocity appears here only as a hidden variable. For example, when the range of velocities in the inset is in the irregular region, there is a wide spread in the location of the resulting points. If we also allow initial velocities from the semiregular region, as happens in the main figure, then the data points are localized around a specific zone that is darker in the figure. This is consistent with an essential independence of these variables when the initial velocities are outside of the irregular region. The number of collision data points in the main figure and in the inset are equal.

Next we discuss the relevant scattering variables of the problem. In Fig. 9 we show the irregular behavior of the exit angle as a function of the normalized initial particle velocity. The low energy particles, with velocities less than 5.3, have an irregular exit angle in a wider range of values. When we plot the distribution of these exit angles, we find a wide pattern centered around an angle of about 0.45 rad. This can be seen in the inset of Fig. 9. Particles with incident velocities larger than 5.3, that show semiregular behavior, also contribute strongly to this peak. The corresponding histograms for these regions are displayed in Fig. 10, with the left histogram associated with the irregular region, and the right one with the semiregular region. Both histograms show a peak for an exit angle around 0.45 rad. For low energy incident particles we obtain a wider range of output angles.

In Fig. 11 we show the exit velocity as a function of input velocity. The region with input velocity less than 5.3 is quite irregular, and it is consistent with the previous figures. When we increase the input velocity, the exit velocity grows and the fluctuations are around a line with a slope of almost 45°. In this figure it is noticeable that there are large jumps for input velocities between 16.7 and 19. The left inset is an amplification for low input velocities. The right inset shows the corresponding histogram for the exit velocities. Here we notice that there are isolated peaks or gaps in this distribution.

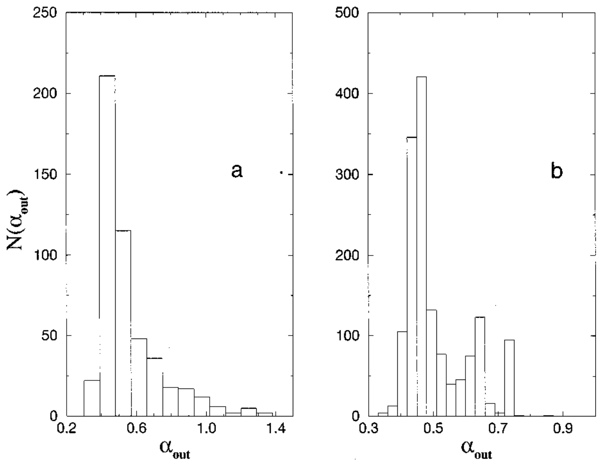

FIG. 10. Histograms of the data $N(\alpha_{out})$ shown in the inset of Fig. 9 that separate irregular and semiregular regions. Both histograms have a peak close to $\alpha_{out}=0.45$ rad. The irregular region histogram is shown in (a). It covers a wider range of output velocities than the semiregular region shown in histogram (b). The bin sizes taken for the histograms are 3% of the full range in α_{out}.

The histograms shown in Fig. 12 are directly related to the data shown in Fig. 11. The left histogram corresponds to the data given in the inset of Fig. 11, while the right one corresponds to the main plot. In both analyzed histograms the fluctuations are around the line with slope $\pi/4$, with data points on this line labeled by the variable v. The variables

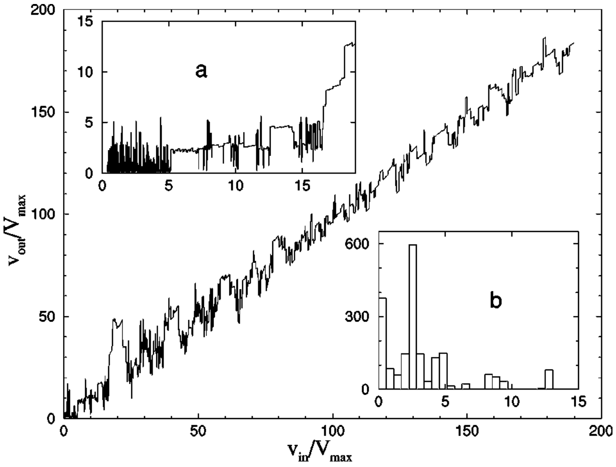

FIG. 11. In the main figure we show the exit velocity vs input velocity for 6000 particles for a wide range of initial velocities. Inset (a) has the same coordinates, but for 2000 input velocities. In inset (a) the irregular region is more detailed, and between 0 and 15 the coarse averaged slope is small, while outside this range the averaged slope is close to $\pi/4$. We use the latter result in the histogram of Fig. 12. The exit velocity histogram is shown in inset (b). Notice the isolated peaks in the distribution.

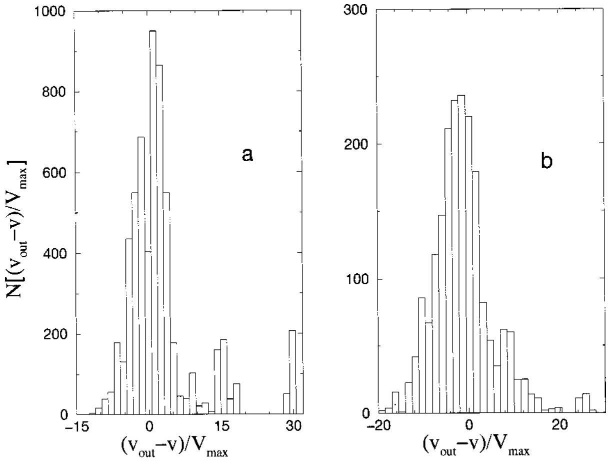

FIG. 12. Histogram of the $N(v_{\rm out}-v)/V_{\rm max}$ data. (a) corresponds to the data given in inset of Fig. 11(a), and (b) to the data shown in the main plot. The fluctuations are analyzed around the line with slope $\pi/4$, and are labeled by the variable v. Here $v_{\rm out}$ is the real output velocity of the particles. We surmise that some of the isolated peaks present may be connected with the exit energy gap regions.

$V_{\rm max}$ and $v_{\rm out}$ are the maximum disk velocity and the real output velocity of the particles, respectively. One important feature of these histograms is that they appear to be directly related to the isolated peaks mentioned before. Here the effect is more prominent for the irregular region of input velocities. The effect remains, even if we make the velocity equal, but with different initial phases. This is equivalent to carrying out a phase average in the interval $(0,2\pi)$. The gaps in the output velocities are also gaps in output energy. These results indicate that there are output energy regions that the particle cannot explore, leading to *forbidden* energy regions. In the inset at the top of Fig. 11, we note that the exit velocities have a peak when the input velocities are close to 19. For the range of velocities between 23 and 60, the energy gaps were not seen. This is why the gaps are wider at the bottom in the inset of Fig. 11. If we increase the range of input velocities, as in the main figure, then there appear narrow gaps related to different velocity contributions.

We have also carried out a basic fractal analysis of a 10 000-particle system. The idea was to extend the analysis of Ref. [5] to two dimensions. We determined the plane boundary of initial conditions (x_0^-,α_0), which separates the particles into the ones that go upwards from the ones that go downwards. We plotted a figure with black squares representing the initial conditions of particles which exit upwards, and empty squares belonging to the ones that go downwards. We obtained 1.86 as the fractal dimension. We do not show these results since they are typical of chaotic scattering problems. We carried out this quantitative analysis to make sure that all the qualitative generic properties of a chaotic scattering system applied. Although all the results are quantitatively different, as one should expect, we did not find a significant change in the general qualitative behavior described above.

Finally, we note that the model we are considering here does not conserve energy, and we are also interested in understanding how energy is added or subtracted from the disk to the colliding particles. One possibility is to take the initial velocities distributed by a Gaussian function, just as in the classical statistical mechanics Maxwell velocity distribution. We then chose a beam of particles with this velocity distribution with a given standard deviation σ, or inverse temperature. Then we studied the evolution of the distribution of exit velocities. We did the analysis at low, intermediate, and high beam energies. The results are shown in Fig. 13. In all of these figures, the continuous line curve represents the Gaussian distribution fit to the beam of incident particle velocities. The histogram is the distribution of exit velocities after scattering. We note that the Gaussian distribution is maintained *only* for high energies (right-bottom figure), but for low or medium energies the exit velocities cannot be fitted to a simple Gaussian. At low energies, when the incident velocities are in the irregular region (left-top figure), however, most particles concentrate about a Gaussian-like distribution, with smaller mean and σ. These latter results indicate that the beam loses energy, and that it has some kind of stochastic cooling.

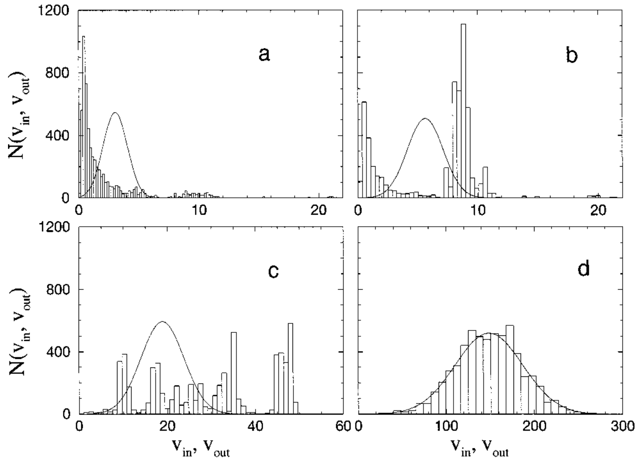

FIG. 13. Each of the four figures was produced from a beam of particles with a Gaussian initial velocity distribution, denoted by a continuous line in the figures. The histograms of $N(v_{\rm in})$ or $N(v_{\rm out})$ were produced from the exit velocities after scattering the oscillating disks. Each figure has a different mean and standard deviation. In (d) we see that the Gaussian distribution is preserved but only for high energies. In the irregular exit velocity region (a), the exit distribution is concentrated about a Gaussian-like distribution with smaller mean and σ. This result can be interpreted as some kind of stochastic cooling. (b) and (c) correspond to intermediate energy regimes where the exit distribution is not Gaussian.

V. CONCLUSIONS

In the present paper we considered the complex dynamics of a particle that scatters from two periodically oscillating disks with a variety of initial conditions. We found that the dynamics has regular and irregular behavior that we analyzed in some detail. This model is in a sense a *dynamical extension* of the well known Lorentz gas [29]. Although the model studied here is perhaps the first dynamic chaotic scattering analysis, several of the results we described are similar to those found in chaotic static scatterers. There are, however, some important unexpected differences in the results obtained. Among the most interesting and surprising results presented in this paper are the energy gaps found in the exit energy. This result indicates that there is an important energy absorbing mechanism, directly related to the nature of the classical dynamics of the problem. We found that the markedly irregular dynamics appears when the particles have velocities on the order of the disk velocities. It is within this energy range that the energy gaps appear. For a larger particle energy the dynamics simplifies, for the oscillating disks appear as if they were at rest.

Another important difference from the dynamics of chaotic static scatterers has to do with the energy gained or lost by the beam of particles. As a test, we took a Maxwell-like distribution of initial velocities, and found that only in the large energy regime, where the disk is essentially seen at rest by the particles, the Gaussian distribution of exit velocities is preserved. Otherwise, there are important changes in the exit velocity distributions for low velocities.

In this paper we considered that the disks do not absorb energy from the colliding particles. Including energy gained or lost by the disks is necessary in order to mimic the effect of temperature in the model. We intend to include this effect in the model elsewhere. The very interesting questions raised by the quantum mechanical treatment of the model introduced here are left for the future.

ACKNOWLEDGMENTS

The work by A.A. was partially supported by DGAPA-UNAM Grant No. IN-105595, and the work by J.V.J. was supported in part by NSF Grant No. DMR-95-21845.

APPENDIX

In this appendix we write down the explicit expressions for the parameters defined in the main body of the text. In order to obtain the values of the parameters $\tilde{A}$, $\tilde{B}$, and $\tilde{C}$ of Sec. II, we use Fig. 2, and ask that the parabolic curve cross through the points $[(m/2)\,T, X_e+A]$ and $[[m+1)/2]T, X_e-A]$, where X_e is the equilibrium position of the center of the disk, and A is the oscillation amplitude. When this is done, we obtain the following expressions:

$$\tilde{A}=\text{free parameter}\,,$$

$$\tilde{B}=(-1)^m\frac{2A}{\pi}+\left(\frac{\tilde{A}}{\omega}\right)[2\Phi_0-\pi(1+2m)], \tag{A1}$$

$$\tilde{C}=X_e+(-1)^{m+1}A(1+2m)+(-1)^m\frac{2A\Phi_0}{\pi}+\left(\frac{\tilde{A}}{\omega^2}\right)[\Phi_0^2+m\pi^2(1+m)-\pi\Phi_0(1+2m)].$$

$\tilde{A}$ is the curvature in the saw tooth, which is associated with the disk acceleration.

The derivation of the parameters a_0, a_1, a_2, a_3 and a_4 appearing in Eq. (7) is a straightforward, and here we just cite the results. We evaluate Eq. (1) at $t=t_{n+1}$ and then substitute the result into Eq. (6). Then we obtain Eq. (7) with the following coefficients:

$$a_0=x_n^2+v_n^2t_n^2+\tilde{C}^2-2x_nv_{nx}t_n+2x_n\tilde{C}-2v_{nx}\tilde{C}t_n+y_n^2-2y_nv_{ny}t_n-1,$$

$$a_1=-2v_{nx}^2t_n+2\tilde{B}\tilde{C}+2x_nv_{nx}+2x_n\tilde{B}-2v_{nx}\tilde{B}t_n+2v_{nx}\tilde{C}-2v_{ny}^2t_n+2y_nv_{ny}\,,$$

$$a_2=v_n^2+\tilde{B}^2+2\tilde{A}\tilde{C}+2x_n\tilde{A}-2v_{nx}\tilde{A}t_n+2v_{nx}\tilde{B}, \tag{A2}$$

$$a_3=2\tilde{A}\tilde{B}+2v_{nx}\tilde{A},$$

$$a_4=\tilde{A}^2.$$

[1] For reviews, see E. Ott and T. Tél, Chaos **3**, 417 (1993), and references therein.

[2] U. Smilansky, in *Chaos and Quantum Physics*, edited by M. J. Giannoni *et al.* (North-Holland, New York, 1992).

[3] T. Tél, in *Directions in Chaos*, edited by Bai-lin Hao (World Scientific, Singapore, 1990), Vol. 3.

[4] J.-M. Petit and M. Hénon, Icarus **66**, 536 (1986); M. Hénon, La Recherche **20**, 419 (1989).

[5] D. W. Noid, S. Gray, and S. A. Rice, J. Chem. Phys. **84**, 2649 (1986).

[6] B. Eckhard and C. Jung, J. Phys. A **19**, L829 (1986).

[7] S. Bleher, E. Ott, and C. Grebogi, Phys. Rev. Lett. **63**, 919 (1989); S. Bleher, C. Grebogi, and E. Ott, Physica D **46**, 87 (1990).

[8] B. Eckhardt, J. Phys. A **20**, 5971 (1987).

[9] S. Bleher, C. Grebogi, and E. Ott, Physica D **46**, 87 (1990).

[10] H. J. Korsh and A. Wagner, Comput. Phys. **5**, 497 (1991).

[11] J. V. José, C. Rojas, and E. Saletan, Am. J. Phys. **60**, 587 (1992).

[12] N. Meyer *et al.*, J. Phys. A **28**, 2529 (1995).

[13] For a review, see, e.g., C. W. J. Beenakker and H. van Houten, Solid State Phys. **44**, 1 (1991).

[14] D. Weiss *et al.*, Phys. Rev. Lett. **66**, 2790 (1991); **70**, 4118 (1993).

[15] R. Schuster *et al.*, Phys. Rev. B **50**, 8090 (1994).

[16] C. M. Marcus, A. J. Rimberg, R. M. Westervelt, P. F. Hopkins, and A. C. Gossard, Phys. Rev. Lett. **69**, 506 (1992).

[17] A. M. Chang, H. U. Baranger, L. N. Pfeiffer, and K. W. West, Phys. Rev. Lett. **73**, 2111 (1994).

[18] A. M. Chang, H. U. Baranger, L. N. Pfeiffer, K. W. West, and L. V. Chang, Phys. Rev. Lett. **76**, 1695 (1996).

[19] J. A. Folk, S. R. Patel, S. F. Godijn, A. G. Huibers, S. M. Cronenwett, C. M. Marcus, K. Campman, and A. C. Grossard, Phys. Rev. Lett. **76**, 1699 (1996).

[20] R. P. Taylor *et al.*, Phys. Rev. Lett. **78**, 1952 (1997).

[21] C. W. J. Beenakker and H. Van Houten, Phys. Rev. Lett. **63**, 1857 (1989).

[22] M. L. Roukes and O. L. Alerhand, Phys. Rev. Lett. **65**, 1651 (1990).

[23] E. M. Baskin *et al.*, Pis'ma Zh. Eksp. Teor. Fiz. **55**, 649 (1992) [JETP Lett. **55**, 678 (1992)].

[24] M. Fließer, G. J. O. Schmidt, and H. Spohn, Phys. Rev. E **53**, 5690 (1996).

[25] T. Geisel, R. Ketzmerick, and O. Schedletzky, Phys. Rev. Lett. **69**, 1680 (1992).

[26] R. Fleischmann, T. Geisel, and R. Ketzmerick, Phys. Rev. Lett. **68**, 1367 (1992); Europhys. Lett. **25**, 219 (1994).

[27] A. J. Lichtenberg and M. A. Lieberman, *Regular and Stochastic Motion* (Springer-Verlag, New York, 1983), p. 194.

[28] A. Brahic, Astron. Astrophys. **12**, 98 (1971).

[29] E. H. Hauge, in *Transport Phenomena: Sitges School of Statistical Physics, Sitges, Barcelona, Spain, 1974*, edited by G. Kirczenow and J. Marro, Lecture Notes in Physics Vol. 31 (Springer, Berlin, 1974); H. van Beijeren, Rev. Mod. Phys. **54**, 195 (1982).